JOURNAL OF SPACECRAFT AND ROCKETS
Vol. 31, No. 4, July–August 1994

Gasdynamic Approach to Small Plumes Computation

L. Genkin* and M. Baer†
Soreq NRC, Yavne 70600, Israel
and
J. Falcovitz‡
Technion, Haifa 32000, Israel

The semiinverse marching characteristics scheme (SIMA) was extended to treat rotational flows; it is applied to computation of free plumes, starting out from nonuniform nozzle exit flow that reflects substantial viscous effects. Since measurements of exit flow in small nozzles (exit diameter of several millimeters) are typically unavailable, the exit plane flow is approximated by introducing a power-law interpolation (PLI) between the exit plane center and lip values. Exit plane flow variables thus approximated are Mach number, pressure, flow angle, and stagnation temperature. This choice is guided by gasdynamic considerations of exhaust flow from small nozzles into vacuum. The PLI is adjusted so as to obtain a match between computations and measurements at intermediate range from the nozzle. Computed plumes were found to be in good agreement with three different sets of small plume experiments. Comparative computations were performed using two alternate methods: the Boynton-Simons point-source approximation, and SIMA computation that started out from a uniform exit flow. It is demonstrated that for small nozzles having an exit flow dominated by viscous effects, the combined SIMA/PLI computational method is reasonably accurate and is clearly superior to either of the two alternate methods.

Nomenclature

a = speed of sound, *m/s*
C_o = streamlines corresponding to θ
$C_\pm$ = characteristic lines corresponding to $(\theta \pm \mu)$
M = Mach number
P = pressure, *M P a*
P_t = Pitot pressure, *M P a*
R = nozzle radius, *mm*
T = temperature, *K*
V = velocity, *m/s*
V_{lim} = limiting (maximum) gas velocity, *m/s*
W = molecular weight, *kg/kmole*
(X, Y) = Cartesian coordinates (Y is axis of symmetry), *mm*
θ = inclination of flow velocity vector relative to X axis
μ = Mach angle, $\sin \mu = M^{-1}$
γ = specific heats ratio
Γ = $[(\gamma + 1)/(\gamma - 1)]^{1/2}$
ρ = density, *kg/m*^{3}
(η,ξ) = length coordinates along $C_\pm$ characteristic lines, *mm*
ν = Prandtl-Meyer function $\nu(M) = \Gamma \arctan [\Gamma^{-1} (M^2 - 1)^{1/2}] - \arctan [(M^2 - 1)^{1/2}]$

Indices

s = stagnation property
c = chamber conditions
a = pertaining to nozzle axis (at exit plane)
e = pertaining to nozzle exit plane
l = pertaining to nozzle lip (at exit plane)
t = pertaining to nozzle throat
w = pertaining to nozzle wall (at exit plane)

Received Nov. 18, 1992; revision received March 8, 1993; accepted for publication March 8, 1993. Copyright © 1994 by the American Institute of Aeronautics and Astronautics, Inc. All rights reserved.

*Senior Scientist, Chemical Reactions Section. Member AIAA.
†Professor and Section Leader, Chemical Reactions Section.
‡Associate Professor, Faculty of Aerospace Engineering. Member AIAA.

I. Introduction

KNOWLEDGE of the structure of rocket exhaust plumes in space is necessary for the analysis of engineering problems related to plume impingement such as heating, contamination, plume induced forces, surface degradation, and charging.[1]

Nozzle boundary layers influence those regions of the plume that are far from the axis, especially in small nozzles. It is an important factor for many applications, particularly since the boundary layer enhances plume spreading to large angles. Spacecraft surfaces may thus be subjected to undesirable forces, heat loads, or contamination which can reduce the lifetime of the spacecraft or impair the functioning of some vital subsystems.

The purpose of this paper is to present a computational scheme for rocket exhaust plumes which yields good agreement with experimental data at the intermediate range of several times $10R_e$ and large angles from the plume's axis, particularly in small thrusters where the nozzle boundary layer dominates the flow at the nozzle exit plane.

An experimental way for analyzing spacecraft plume flowfields and impingement effects is studying rocket exhaust plumes under laboratory conditions. However, since enormous pumping capabilities are necessary to maintain high vacuum during thruster firing, this approach is restricted to small thrusters.[1]

Turning to theoretical analysis, an analytic approximation suggested by Boynton[2] and Simons[3] is often employed for estimating the far field in a plume flow. The basic idea of this nonisotropic point-source model is that the continuum flowfield outside of the nozzle is divided into an isentropic core expansion region and a boundary-layer expansion region. Far from the nozzle all streamlines are assumed to be straight and to emanate from a virtual origin at the center of the nozzle exit plane.

A reasonable agreement between experimental data and the Boynton-Simons model was found.[4-8] However, the application of the analytical Boynton-Simons approximation to regions of large angles from the plume axis yielded densities smaller by as much as a factor of 10 relative to experiments.[4,8] Moreover, semiempirical expressions for transverse profiles of density for the isentropic core expansion agreed with the experimental results only at large distances from the nozzle of around $50R_e$.[5] Thus, improved numerical computations are called for to enable

the analysis of plume flowfields at intermediate range and large side angles, where available analytic approximations are inaccurate.

Considering numerical schemes, there exist numerous methods for computing nozzle and plume flows in the continuum regime,[9-13] or as rarefied flow.[14,15] The most suitable continuum computing method (particularly for resolving the expansion flow about the nozzle lip) is probably the classical method of characteristics (MOC), adapted to rotational flows.[16] For the present study, we have put together a particular MOC version; it is the semiinverse marching algorithm (SIMA),[17] which has been extended to rotational flow.

There are basically two alternate approaches in applying the MOC to plume flow computation. In the first, represented by the CONTAM code,[11] the computation commences at a sonic surface located near the nozzle throat and proceeds through the expansion segment of the nozzle directly into the plume. In the second approach, the computation starts out from a (presumably known) flow at the nozzle exit plane, which serves as initial conditions for the MOC constructive solution of the plume flowfield.

A major difference between these two approaches lies in the method by which they treat viscous effects in the nozzle flow. In the first approach, the nozzle boundary-layer buildup is accounted for by introducing a boundary-layer-displaced nozzle contour.[11] In the second approach, nozzle viscous effects are reflected by the degree of nonuniformity of the flow at the nozzle exit plane. (We note that in any MOC computation, viscous effects in the plume itself are ignored.)

Although the displaced nozzle contour idea is a valid approximation for medium or large thrusters (100 N or higher[11]), it is inadequate for small thrusters ($\approx$ 1 N), where virtually the entire nozzle exit flow is influenced by viscous effects.

Exit plane flow measurements in small nozzles exhausting into vacuum are generally unavailable, so that there is no way to obtain accurate information on the exit plane flow distribution. The next best alternative might be a viscous nozzle flow computation, using an available scheme such as VNAP2.[13] However, since experimental verification—depending on measurements performed far downstream from the nozzle—would invariably be indirect, we opted for a different approach. The basic idea is to employ a parametric approximation to the actual (unknown) exit plane flow, choosing the parameters so as to obtain a match between computed and measured plume flows. This results in a hybrid engineering model for computing small plume flows: the nozzle exit flow is approximated by a monotonic power-law interpolation, which constitutes the initial conditions for an accurate MOC construction of the plume flowfield.

The basic idea on which the power-law interpolation (PLI) is founded is the following. Assuming inviscid nozzle expansion flow, an optimal design would render a nearly uniform flow at the exit plane. Because of viscous effects, the actual flow distribution would typically exhibit a monotonic reduction in Mach number, stagnation pressure, and stagnation temperature near the nozzle wall. A typical functional form capturing the essential features of such variation would be the "power law" $F(X) = A - (A - L)\,[X/R_e]^N$, where $[X/R_e]$ is the normalized exit plane radius; A and L are the values of the flow variable at the axis and lip, respectively; and $N > 1$ is a power. In the present PLI version, the PLI approximation was actually applied to Mach number, pressure, flow angle θ, and stagnation temperature. The gasdynamic reasoning leading to this particular choice of exit flow variables is brought in Sec. III below.

Consequently, we regard the PLI as an interpolation between the (presumably known) value of a flow variable at the center of the exit plane (axis) and its value at the nozzle lip. The magnitude of the power N expresses the degree by which viscous effects influence the exit plane flow: a lower N corresponds to a thicker boundary layer, whereas a higher N corresponds to a more uniform exit flow and a thinner boundary layer.

The plan of the paper is as follows. In Sec. II, we introduce the SIMA scheme extended to rotational flows and the confirmation of its mathematical accuracy. In Sec. III, we present the PLI approximation to exit plane flow, and the methodology for the determination of the PLI coefficients. In Sec. IV, computed SIMA/PLI plumes are compared to experimental data; this is done for three different sets of small plume experiments. To relate SIMA/PLI computations to alternate theoretical approaches, we also present two additional plume computations. The first is SIMA integration that starts out from a uniform exit flow, and the second is a Boynton-Simons plume approximation. Also, along with the computational results, we present an assessment of their sensitivity to PLI coefficients. In Sec. V, final comments and conclusions are given, followed by a list of references.

II. The Computational Scheme

Rocket exhaust plumes in outer space are commonly idealized as stationary shockless supersonic flow of a free jet consisting of an inviscid perfect gas, expanding into a zero-pressure ambiance. Under these idealizations, the plume flowfield is most appropriately computed by some method of characteristics (MOC) scheme. Assuming further that the plume is axisymmetric, the MOC construction is performed in the two-dimensional space (X, Y) corresponding to a plane passing through the plume axis of symmetry (Y).

Because of nonuniformity of rocket exit plane flow, related to both nonuniform nozzle expansion and viscous effects (boundary layer), the free expansion flow is idealized as being isentropic along streamlines, while having a nonuniform entropy across streamlines (i.e., rotational flow). Hence, the computational grid consists of the two characteristic lines $C_\pm$ and the streamlines C_o. A standard reference for such schemes is Zucrow and Hoffman,[16] and a typical application to rocket exhaust plumes computation is the CONTAM code.[11]

Even though there are numerous MOC schemes and codes reported in the literature, we chose to formulate our own version: the semiinverse marching algorithm (SIMA[17]). The considerations leading to this choice are presented in detail.[17] The SIMA scheme has the advantage of generating a relatively regular solution grid (unlike the typically irregular grid resulting from integration along continuous $C_\pm$ characteristic lines), combined with accurate computation of a centered rarefaction wave (Prandtl-Meyer flow).

The original SIMA scheme[17] was restricted to nonrotational (homentropic) flows. Here we present an extension of SIMA to rotational flows, by adding to the governing equations two relations that express the constancy of entropy and stagnation enthalpy along streamlines. We start the derivation of this extended SIMA scheme by considering the compatibility relations for axisymmetric stationary rotational supersonic flow of an inviscid gas [Eqs. (17.3), (17.32), and (17.33) in Ref. 16].

Along $C_\pm$:

$$\frac{\cos\theta}{MX\cos(\theta \pm \mu)}\,dX + \frac{(M^2-1)^{1/2}}{\rho V^2}\,dP \pm d\theta = 0 \qquad (1a)$$

Along C_o:

$$\rho V\,dV + dP = 0 \qquad (1b)$$

Along C_o:

$$dP - a^2\,d\rho = 0 \qquad (1c)$$

where $C_\pm$ and C_o are determined by the following geometrical relations:

$$C_\pm: \quad \frac{dY}{dX} = \tan(\theta \pm \mu) \qquad (2a)$$

$$C_o: \quad \frac{dY}{dX} = \tan(\theta) \qquad (2b)$$

Thus, there is one compatibility relation valid on each characteristic line $C_{\pm}$, and two relations valid along the streamline C_o; a total of four differential relations involving the four flow variables ρ, p, θ, and V. In addition, we have the three geometrical relations [Eq. (2)] that enable the construction of the computational grid in the (X, Y) plane.

In compliance with the SIMA scheme, the flow variables P and θ in the compatibility relations [Eq. (1a)] are replaced by the Riemann invariants $(\nu \pm \theta)$. It was also found convenient to express the relations along streamlines in terms of stagnation variables P_s, T_s. Using the standard relations for isentropic flow of perfect gas,

$$d\nu = \frac{(M^2 - 1)^{1/2}}{M\,(1 + [(\gamma - 1)/2]\,M^2)}\,dM \tag{3a}$$

$$\frac{dV}{V} = \frac{1}{2}\frac{dT_s}{T_s} + \frac{dM}{M} - \frac{\gamma - 1}{2}\frac{M}{(1 + [(\gamma - 1)/2]\,M^2)}\,dM \tag{3b}$$

$$\frac{dP}{P} = \frac{dP_s}{P_s} - \frac{\gamma M}{(1 + [(\gamma - 1)/2]\,M^2)}\,dM \tag{3c}$$

we readily derive from Eq. (1) the following set of four differential relations:

$$C_+: \quad d(\nu - \theta) = \frac{\cos\theta}{MX\cos(\theta + \mu)}\,dX + \frac{(M^2 - 1)^{1/2}}{\gamma M^2}\frac{dP_s}{P_s} \tag{4a}$$

$$C_-: \quad d(\nu + \theta) = \frac{\cos\theta}{MX\cos(\theta - \mu)}\,dX \tag{4b}$$

$$+\frac{(M^2 - 1)^{1/2}}{\gamma M^2}\frac{dP_s}{P_s} \tag{4c}$$

$$C_o: \quad dP_s = 0 \tag{4d}$$

$$C_o: \quad dT_s = 0$$

We note that the stagnation pressure P_s is coupled with the compatibility relations [Eqs. (4a) and (4b)], while the stagnation temperature T_s is not coupled with those relations. By virtue of this fact, the system [Eq. (4)] reduces to a set of three coupled differential relations for the flow variables $(\nu + \theta)$, $(\nu - \theta)$, P_s, plus a single relation [Eq. (4d)] for T_s. Referring to the alternate constructive diagrams in Figs. 1 and 2, a finite difference scheme for integrating these relations, analogous to the corresponding homentropic scheme [Ref. 17, Eqs. (1) and (2)], is the following:

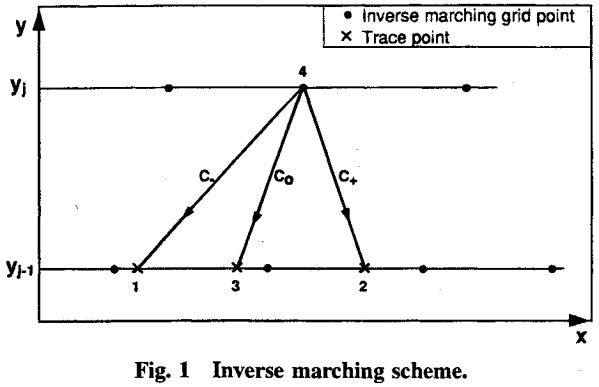

Fig. 1 Inverse marching scheme.

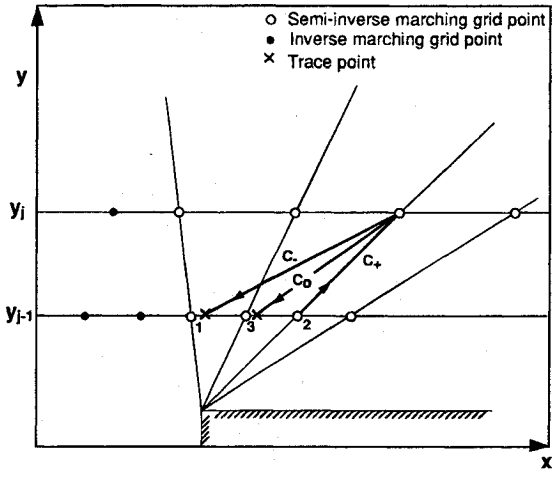

Fig. 2 Semiinverse marching scheme.

$$C_+: \quad (\nu - \theta)_4 = (\nu - \theta)_2 + \frac{\sin\mu_{24}\cos\theta_{24}}{X_{24}}\Delta\eta_{24} \tag{5a}$$

$$+\frac{(M_{24}^2 - 1)^{1/2}}{\gamma M_{24}^2}\frac{(P_{s4} - P_{s2})}{P_{s24}} \tag{5b}$$

$$C_-: \quad (\nu + \theta)_4 = (\nu + \theta)_1 + \frac{\sin\mu_{14}\cos\theta_{14}}{X_{14}}\Delta\xi_{14} \tag{5b}$$

$$+\frac{(M_{14}^2 - 1)^{1/2}}{\gamma M_{14}^2}\frac{(P_{s4} - P_{s1})}{P_{s14}} \tag{5c}$$

$$C_o: \quad P_{s4} = P_{s3} \tag{5d}$$

$$C_o: \quad T_{s4} = T_{s3}$$

where the centered values $(\cdot)_{14}$ and $(\cdot)_{24}$ are defined as follows. For the primary flow variables $(\nu \pm \theta)$, P_s, T_s (and also for X), the centered values are the arithmetic mean of the respective point values. For the dependent variables μ, θ, ν, and M, the centered values are obtained by computing them as functions of the centered values of the respective primary variables, according to the relations:

$$\nu = \frac{1}{2}[(\nu + \theta) + (\nu - \theta)] \tag{6a}$$

$$\theta = \frac{1}{2}[(\nu + \theta) - (\nu - \theta)] \tag{6b}$$

$$\nu(M) = \Gamma\arctan\left[\Gamma^{-1}(M^2 - 1)^{1/2}\right] - \arctan\left[(M^2 - 1)^{1/2}\right] \tag{6c}$$

$$\Gamma = \left[\frac{\gamma + 1}{\gamma - 1}\right]^{1/2} \tag{6d}$$

$$\mu = \arcsin(M^{-1}) \tag{6e}$$

Note that the definition of M as function of ν by Eq. (6c) is an implicit one; since $\nu(M)$ is a monotonic function for $M > 1$, the inverse function $M(\nu)$ is single-valued and it is readily computed by standard Newton-Raphson iterations.

The finite difference scheme defined by Eqs. (5) and (6) has to be supplemented by geometrical relations between the new marching point (4) and the old points (1), (2), and (3). Assuming that the segments (1–4), (2–4), and (3–4) of the characteristic lines are straight, these relations are

$$C_+: \quad Y_j - Y_{j-1} = (X_4 - X_2) \tan(\theta_{24} + \mu_{24}) \tag{7a}$$

$$C_-: \quad Y_j - Y_{j-1} = (X_4 - X_1) \tan(\theta_{14} - \mu_{14}) \tag{7b}$$

$$C_o: \quad Y_j - Y_{j-1} = (X_4 - X_3) \tan(\theta_{34}) \tag{7c}$$

There are two versions of the integration scheme: the inverse marching version and the semiinverse marching one. In the inverse marching case (Fig. 1), Eq. (5) along with the ancillary relations [Eq. (6)] and the geometrical relations [Eq. (7)] are solved by repeated iterations for the unknown flow variables $(\nu + \theta)_4$, $(\nu - \theta)_4$, P_{s4}, T_{s4}, plus the unknown trace point coordinates X_1, X_2, and X_3. The values of flow variables at the three trace points are obtained by linear interpolation using the corresponding values at adjacent old grid points. In the semiinverse marching case (Fig. 2), Eq. (5) along with the ancillary relations [Eq. (6)] and the geometrical relations [Eq. (7)] are also solved by repeated iterations for the unknown flow variables $(\nu + \theta)_4$, $(\nu - \theta)_4$, P_{s4}, T_{s4}, plus the unknown trace point coordinates X_1, X_3, and the new grid point X_4. Again, the values of flow variables at the two trace points are obtained by linear interpolation using the corresponding values at adjacent old grid points. Experience has shown that the repeated iterations generally converged after several rounds.

To enable computation in regions located at high polar angles to plume axis, the grid scheme was generalized to a rectangular pattern as shown in Fig. 3. This is done by designating a particular C_+ characteristic line as the "grid diagonal," separating grid lines of constant Y from grid lines of constant X. The finite difference schemes for grid points located on constant X lines is analogous to those for the constant Y points, with the obvious interchange of X and Y as known and unknown coordinates in the geometrical relations [Eq. (7)].

The next stage in constructing our SIMA/PLI method is to combine the rotational SIMA scheme with the PLI approximation to the exit flow of small nozzles. However, since the validation of SIMA/PLI depends on comparison with experiments, we perform a preliminary confirmation of the rotational SIMA scheme, aimed at demonstrating its mathematical accuracy and convergence.

Since we are not aware of mathematically accurate solutions to rotational plume flows, we opted for a related, albeit not identical, expansion flowfield, i.e., the inviscid supersonic expansion of a perfect gas in a contoured nozzle. Our specific sample nozzle had a geometrical area ratio of 25 corresponding to a nominal exit Mach number of $M_e = 5$ (for $\gamma = 1.4$). The ratio of length to throat radius was 16 and the contour was chosen so that the wall divergence angle increased monotonically from zero at the throat to 28.7 deg at the nozzle lip. Denoting by X_n and Y_n the radial and axial coordinates (normalized to $X_n = 1$ at the throat), the contour was given by

$$X_n(Y_n) = \exp[1.991 \sin^2(Y_n/14.315)], \qquad 0 \le Y_n \le 16 \tag{8}$$

The throat Mach number was assigned a nearly sonic value ($M_t = 1.05$) and the flow velocity vector at the throat plane (the integration startline) was parallel to the axis. The SIMA scheme in the nozzle was a modified semiinverse marching version: streamlines were continuously extended forward, whereas the two characteristic lines $C_\pm$ were inversely extended. Grid points were obtained at the intersection of each streamline with lines of constant Y.

The accuracy of the nozzle computations was confirmed by the following procedure. Since the flow along each streamlines is isentropic, the Mach number and area ratio must obey the usual isentropic relation along each streamtube. By computing the flow along streamlines from the compatibility relations, we have an opportunity for an independent check: evaluate the area ratio evolution in each streamtube at some chosen Y, and hence the related Mach number; then compare it to the Mach number obtained from the SIMA integration. Actually, we evaluated the area-weighted rms deviation between these two Mach numbers at each nozzle cross section, obtaining for the homentropic case a relative rms deviation at the nozzle exit plane of 0.54% and 0.26% for grids of 50 and 100 streamtubes, respectively.

This test was repeated for rotational flow by assuming the following nonuniform flow at the throat. The Mach number was assumed to vary according to the PLI expression [Eq. (9)], with the power being 4, the axis value being 1.5 and the wall value 1.05. The static pressure was uniform, and the stagnation pressure was obtained from the static pressure and the Mach number according to the standard isentropic relation. The rotational flow rms deviations in the respective cases were 0.62% and 0.32%.

We contend that this result constitutes a confirmation of the convergence and accuracy of the rotational SIMA scheme. The irrotational SIMA[17] was independently confirmed by comparison with direct MOC constructed flows; now, here we have demonstrated that a certain level of agreement is obtained when Mach number from irrotational SIMA is compared to Mach number evaluated from streamtube area ratio. This same procedure renders comparable accuracy levels in the rotational SIMA case. We conclude that the mathematical accuracy of the rotational SIMA scheme is comparable to that of the irrotational scheme. We therefore feel reasonably confident that at the next stage, when SIMA/PLI computations will be compared to

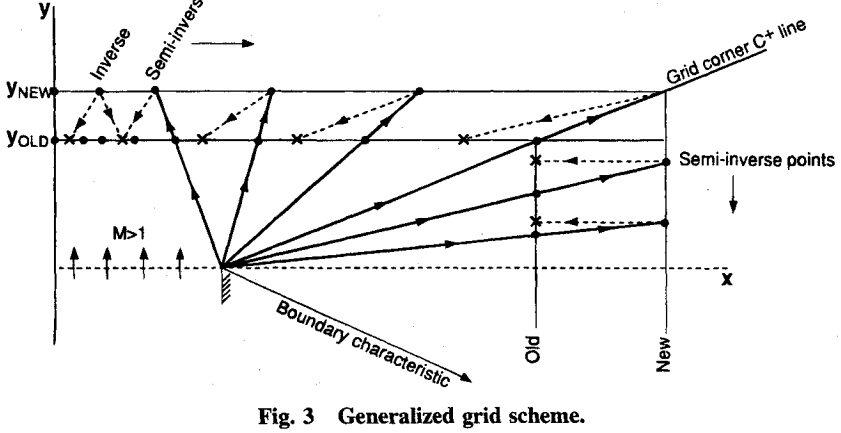

Fig. 3 Generalized grid scheme.

experiments, a numerically converged solution will have a negligible numerical integration error relative to the deviation between computed and measured flow variables.

III. Power-Law Interpolation

The application of SIMA scheme to the marching integration of plume flowfield requires as initial conditions the specification of flow variables across the nozzle exit plane. Aiming at a confirmation of our SIMA/PLI method, we chose to compare our computations particularly with some recent experimental data on attitude control thrusters plumes, obtained by Legge and Dettleff[7] who fired small hydrazine thrusters inside a vacuum chamber simulating the outer space environment. In these experiments, Pitot pressure was recorded at plume points located in the range of 8–32 exit radii from the nozzle. However, no detailed measurements of the flowfield at the exit plane were performed. Other small plume experiments[4,5] were also found lacking in this respect. (This lack of experimental data is understandable considering the small nozzle diameter of several millimeters, and also considering that there is generally no interest in plume interactions at very close range to the nozzle.)

For small thrusters, where viscous effects influence just about the entire flowfield at the exit plane, we propose to overcome this unavailability of experimental data by a PLI for approximating a nonuniform small nozzle exit flow. The key idea is that flow variables are to be approximated by an interpolating power-law function of the exit plane radius, having the following general form:

$$F(X) = F_a - (F_a - F_l)\,[X/R_e]^{N_F} \tag{9}$$

where $F(X)$ denotes some flow variable; F_a and F_l are the values at the nozzle axis and at the nozzle lip, respectively; and N_F is a positive power. Clearly, the resulting plume flowfield will bear out the influence of the degree of nonuniformity of the exit flow, compared to a plume obtained from a uniform exit flow ($F_a = F_l$). In general, the higher the difference ($F_a - F_l$) relative to F_a and the lower the value of N_F, the higher the exit flow nonuniformity.

In principle, the values of F_a, F_l, and N_F are to be determined by somehow matching computations to experimental data. However, our method for determining these coefficients is not based on a formal mathematical fitting procedure, but rather on a series of considerations pertaining specifically to gasdynamics of small nozzle flows exhausting into a zero-pressure ambience.

Consider first the Mach number at the nozzle exit plane. It was shown by Bird[18] that when the nozzle ambience is a vacuum, and when the lip is idealized as a sharp corner, the lip flow velocity is sonic. Physically, this is a manifestation of an accelerating pressure gradient just upstream of the lip. Hence, an appropriate PLI approximation to the exit plane Mach number $M_e(X)$ should have $M_l = 1$. To avoid possible numerical difficulties with gasdynamic functions, we choose a slightly higher value of M_l, typically

$$M_l \approx 1.1 \quad \text{to} \quad 1.2 \tag{10}$$

Computation results exhibited relative insensitivity to actual values of M_l in this range.

We now turn to the exit plane pressure, for which we also apply some intricate gasdynamic reasoning, in order to assist in the determination of the lip pressure value. In this matter, we follow a line of reasoning analogous to that of Smith.[19] We recall that transverse pressure gradients are commonly neglected in boundary-layer analysis. Moreover, an optimal nozzle is designed to render a uniform exit plane flow, including a uniform pressure. Based on these considerations, and naturally subject to specific nozzle design, we assume that ideally the pressure should be uniform in cross-section planes just upstream of the nozzle exit plane. Assuming a completely uniform pressure at the exit plane would not be consistent with the attainment of sonic velocity at the nozzle lip. Rather, the following argument is applied towards estimatinng the pressure at the nozzle lip. The flow adjacent to the nozzle wall is accelerated over a short distance upstream of the lip, from a velocity of about zero to a sonic velocity. Assuming that this acceleration is isentropic (due to negligible wall friction losses over the short distance), and assuming a uniform pressure at the plane where this acceleration commences, the lip stagnation pressure is equal to the static pressure at the point where wall flow velocity is zero. Furthermore, this point being not far upstream of the lip, the pressure there is well approximated by the pressure at the center of the exit plane P_a. Hence, we set the stagnation pressure at the lip equal to P_a. Consequently, the relation between lip and axis value of exit plane pressure is

$$P_l = P_a \left[1 + \frac{\gamma - 1}{2} M_l^2\right]^{-(\gamma/\gamma - 1)} \tag{11}$$

Admittedly, the derivation leading to Eqs. (10) and (11) is of questionable accuracy; we shall later demonstrate that the SIMA/PLI method is relatively insensitive to these assumptions. Having invoked the gasdynamic reasoning leading to the important relations [Eqs. (10) and (11)] for PLI parameters M_l, P_a, and P_l, we present our PLI approximation for the four flow variables M, P, θ, T_{se} as follows:

$$M_e(X) = M_a - (M_a - M_l)\,[X/R_e]^{N_M} \tag{12a}$$

$$P_e(X) = P_a - (P_a - P_l)\,[X/R_e]^{N_P} \tag{12b}$$

$$\theta_e(X) = \theta_a - (\theta_a - \theta_l)\,[X/R_e]^{N_\theta} \tag{12c}$$

$$T_{se}(X) = T_a - (T_a - T_l)\,[X/R_e]^{N_T} \tag{12d}$$

Our PLI approximation to the four flow variables in Eq. (12) calls for the determination of 12 coefficients. However, the actual freedom in assigning appropriate values to these coefficients is drastically reduced when relations Eqs. (10) and (11), along with other considerations are taken into account. Since this is a central feature of our plume computation method, we outline the procedure leading to the determination of the PLI coefficients in some detail.

We always start with the Mach number $M_e(X)$. Its axis value M_a is chosen close to the nominal exit Mach number of the particular thruster (usually somewhat less, perhaps due to boundary-layer-reduced effective area ratio). Since M_l is already given by Eq. (10), the only truly free parameter is the power N_M. We determine the power (and a fine adjustment of M_a) by matching computed and measured flow variables along the plume axis in an intermediate range ($10 < Y/R_e < 100$). It was found that axial variation of flow variables (such as Pitot pressure) is rather sensitive to the power N_M. A higher N_M corresponds to a more uniform exit plane flow and a thinner boundary layer, and vice versa.

We now turn to the pressure $P_e(X)$. Since generally the thruster chamber pressure is measured, then by assuming an isentropic expansion along the nozzle axis, we have the standard isentropic relation between the axis pressure P_a and the axis Mach number M_a. Relation Eq. (11) is then used to determine P_l. Again, the power N_P is the only truly free PLI parameter. When Pitot pressure measurements are available, we determine this parameter by matching computed and measured transverse variation of Pitot pressure at some intermediate range (variation with X at constant Y).

The third variable to be considered for PLI is the flow angle $\theta_e(X)$. Since the nozzle is axisymmetric we always set $\theta_a = 90$ deg. Also, assuming the velocity vector just upstream of the

lip to be tangent to the wall, we set $\theta_l = \theta_w$, where θ_w is the nozzle exit wall angle. The only remaining free parameter is again the power N_θ. We normally assign N_θ a value of about 2. We use transverse variation of a measured and computed flow variable as an aid in determining a good value for N_θ.

It is clear from the above outline that the set of PLI parameters for $M_e(X)$, $P_e(X)$, and $\theta_e(X)$ ought to be determined simultaneously. Since as indicated in Sec. II, the distribution of nonuniform stagnation temperature in the exit flow does not affect the flowfield Mach number, nor its streamlines or pressure, the determination of $T_{se}(X)$ is not coupled to the determination of the preceding three flow variables. To sum it up, there are only four coupled PLI coefficients, namely the respective powers and the axis Mach number M_a; they are determined by the axial and transverse matching procedures outlined above. This concludes the major stage of the determination of PLI coefficients; the only remaining variable to be matched is the stagnation temperature.

For the stagnation temperature $T_{se}(X)$, we follow a very simple procedure. Generally, chamber temperature T_c is known (from measurement or by indirect assessment); we then set $T_a = T_c$. As for T_l and N_T, they are determined by matching transverse computed and measured temperature or limiting velocity. In the absence of such measurements, any reasonable guess can be made for T_l and N_T. Note, however, that the uncertainty in stagnation temperature distribution will not affect the streamlines and characteristics map, the Mach number, or the pressure.

Having specified the exit plane distribution of the four variables in Eq. (12), we evaluate the primary flow variables using the perfect gas relations [Eq. 6] plus the standard relation between static and stagnation pressure as function of local Mach number. These constitute the initial conditions required for the construction of the plume flowfield using the SIMA scheme.

IV. Numerical Results and Comparison with Experiments

Aiming at a confirmation of our combined SIMA scheme and PLI approximation of nozzle exit plane flow, we present some detailed comparison of our computations with measured plume flowfields. The experimental studies that were chosen for this comparison are as follows:

(1) Legge and Dettleff's[7] Pitot pressure measurement of hydrazine thruster plumes in a vacuum chamber.

(2) Calia and Brook's[4] measurement of density, mass flux, and limiting velocity in a shock tube driven nitrogen exhaust plume.

(3) Lengrand et al.[5] measurement of density and temperature in an underexpanded nitrogen jet.

In this section, we present separately the comparison of our computations with each set of experiments mentioned above. In particular, we address the question of the sensitivity of SIMA/PLI computations to the various PLI coefficients. It is demonstrated that in most instances computed flow variables are relatively insensitive to the model parameters.

A. Comparison with Legge and Dettleff Experiments

Small thruster plume measurements under conditions that closely approximate outer space environment were recently performed by Legge and Dettleff.[7] Of the three nozzles tested by them, we chose the conical 0.5 N monopropellant hydrazine thruster, since it clearly exhibited shock-free expansion, whereas the divergent segment of the other two (contoured) nozzles tested, contained some oblique shocks (see Figs. 7 and 8 in Ref. 7).

The geometrical data of the conical nozzle was throat radius $R_t = 0.3$ *mm*, exit plane radius $R_e = 2.375$ *mm*, and half-cone angle = 15 deg ($\theta_w = 75$ deg). The tests were performed with hydrazine, for which an average-range molecular weight is about $W = 13$ and the specific heats ratio is $\gamma = 1.4$.[7] The chamber pressure was $P_c = 1.57$ MPa and the chamber temperature was about 1100 *K*. The measurements performed were Pitot pressure and heat flux rate, of which we chose the former for our comparisons. The reason for this choice is that in supersonic flow the Pitot pressure is related to local flow variables as the stagnation pressure behind a stationary normal shock at the local Mach number. The relation between heat flux rate and local flow variables is considerably more involved (due to viscous effects[7]), and hence Pitot pressure is preferable for the purpose of scheme validation.

We now turn to the actual comparison of computational and experimental results. These are presented in Figs. 4–6. In Fig. 4, the variation of Pitot pressure along the plume axis is depicted; in Figs. 5 and 6, we present the transverse variation of Pitot pressure at axial standoff distances of $8R_e$ and $16R_e$, respectively. The value of PLI coefficients with which the computations were performed is indicated on Fig. 4. We note that the stagnation temperature PLI coefficients were omitted in this case, since Pitot pressure measurements are not affected by stagnation temperature (a uniform one was assumed). Three computational curves are presented in each figure. These are as follows:

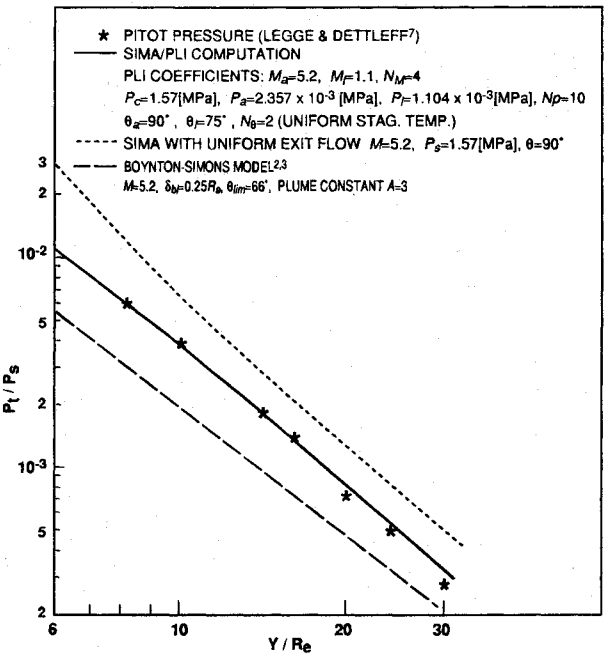

Fig. 4 Comparison of computed and measured Pitot pressure along plume axis ($\gamma = 1.4$).

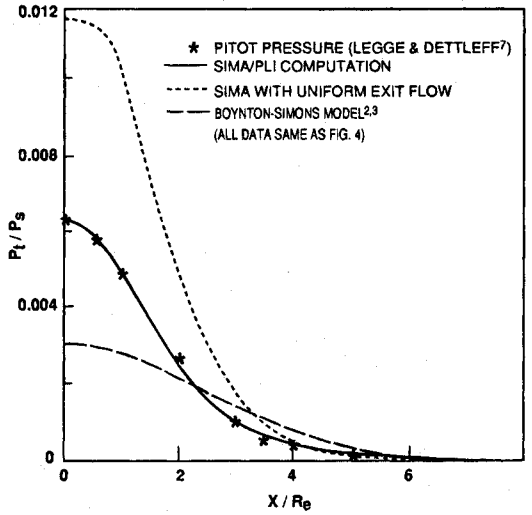

Fig. 5 Comparison of computed and measured Pitot pressure across the plume at $Y = 8R_e$ ($\gamma = 1.4$).

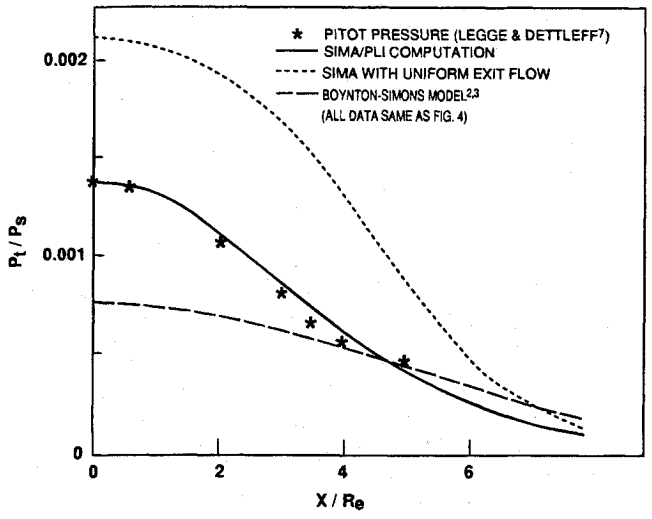

Fig. 6 Comparison of computed and measured Pitot pressure across the plume at $Y = 16R_e$ ($\gamma = 1.4$).

(1) The PLI computation aimed at matching the experimental Pitot pressures.

(2) A uniform exit flow computation, where exit flow variables were set to the PLI axial exit value (including the flow angle, i.e., a parallel uniform exit flow is assumed).

(3) The analytical approximation of Boynton and Simons.[2,3] This classical model was applied to the particular nozzle at hand, with the parameter values as indicated in Fig. 4.

Referring to both axial and transverse Pitot pressure variations (Figs. 4–6), it is apparent that the PLI computations match closely the measurements, while the other two computations do not. We now examine these results in some detail, aiming at illuminating significant features of the various computational schemes.

Turning to the axial variation (Fig. 4), we note that the Boynton-Simons model exhibits a trend of approaching the measurements at increasing range. This is hardly surprising considering the asymptotic nature of this point-source approximation to actual rocket exhaust flows. At the intermediate range of around $30R_e$, though, the Boynton-Simons model is clearly inaccurate.

The uniform SIMA computation is also at disagreement with measurements, clearly demonstrating the significance of approximating the nonuniform exit plane flow by the PLI procedure. There is an important point in the matching of PLI parameters to be considered here. Our chosen axial exit Mach number $M_a = 5.2$ corresponds to an effective isentropic area ratio constituting 46.7% of the geometrical area ratio of 62.7.[7] This corresponds to an effective exit radius of $0.683R_e$, which indicates that the exit plane flow is dominated by viscous effects. The implication is that there is hardly any inviscid core at the exit plane of this small nozzle, and hence the flow at the plume axis, as well as its downstream axial evolution, are affected by the transverse nonuniformity of the exit plane flow. The sensitivity of SIMA/PLI method to M_a was estimated by repeating the computation with $M_a = 5.1$, resulting in about 2% increase in the Pitot pressure. This is a relatively small sensitivity, as a change of the specific heats ratio from $\gamma = 1.40$ to $\gamma = 1.37$ resulted in a 17% change in the axis Pitot pressure.

The transverse cases (Figs. 5 and 6) exhibit a pronounced disagreement between the measurements and both uniform SIMA computations and Boynton-Simons approximation. As for the SIMA computations, the observed results are readily interpreted by noting that at high supersonic Mach number, Pitot pressure tends to be proportional to local density, i.e., roughly proportional to $M^{-2/(\gamma-1)}$. Thus, the exaggerated value of Pitot pressure near the plume axis is attributed to an underestimate of the actual Mach number. Since both uniform and nonuniform SIMA computations start out with equal Mach numbers at the center of the exit plane, this effect is an evidence to the accelerated streamwise increase of plume axis Mach number, caused by the transverse nonuniformity of the exit plane flow. At transverse radius of about $4R_e$ to $5R_e$, the uniform and nonuniform SIMA computations have comparable Pitot pressures and hence comparable Mach numbers. This is interpreted as indicating a higher expansion area ratio in streamtubes of the nonuniform case, relative to the uniform one, which compensates for the exit plane Mach number in the nonuniform flow being lower than that in the uniform flow.

To assess the sensitivity of the transverse distributions to PLI coefficients, we performed several additional computations of transverse Pitot pressure distribution, changing a single coefficient at a time. A change of the flow angle power to $N_\theta = 1$ resulted in a decrease of 13% in Pitot pressure largely at the near range of $Y = 8R_e$ and $X < 3R_e$, and negligible change elsewhere. This is understandable as streamtube divergence at the exit plane has little influence on the flow far from the nozzle. The accuracy of assuming Eqs. (10) and (11) was assessed as follows. We changed the lip Mach number to $M_l = 1.2$ and found negligible change in Pitot pressure. Then we changed the pressure to *uniform*, i.e., $P_l = P_a$ and found a 10% increase in Pitot pressure in the near range of $Y = 8R_e$ and $X < R_e$ with negligible change elsewhere. This result demonstrates an insensitivity of the PLI model to the approximations inherent in Eqs. (10) and (11). In addition, we also checked the influence of the pressure power by changing it to $N_P = 9$, again finding a small decrease of 2% in Pitot pressure in the near range referred to above.

The Mach-number power N_M is a central coefficient in the SIMA/PLI method and its value is to be carefully determined. To demonstrate the sensitivity to this parameter, we repeated the computation with $N_M = 5$. The result was an almost uniform increase in Pitot pressure of about $0.0002P_C$, which constitutes about 3% of the axis Pitot pressure.

B. Comparison with Calia and Brook Experiments

In Figures 7 and 8, the angular profiles obtained by Calia and Brook[4] are reproduced and compared to the SIMA/PLI computation and (in the case of density) to the uniform SIMA

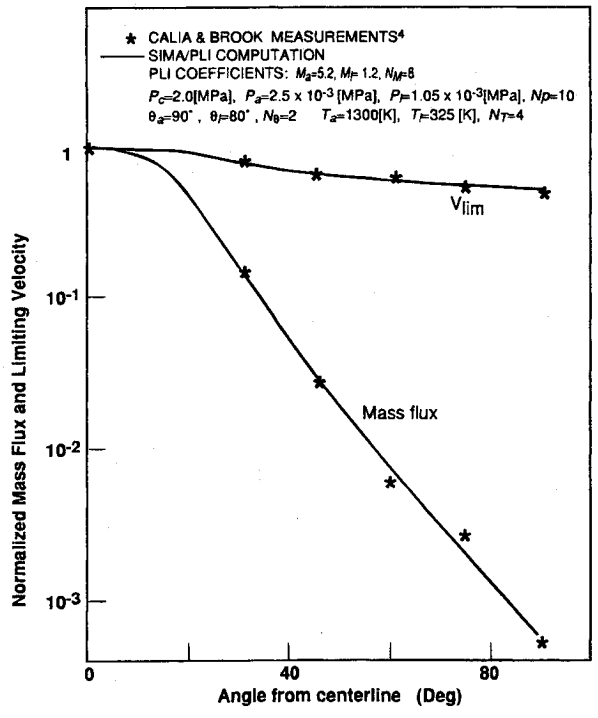

Fig. 7 Comparison of computed and measured limiting velocity and mass flux at polar radius of $92R_e$ ($\gamma = 1.37$).

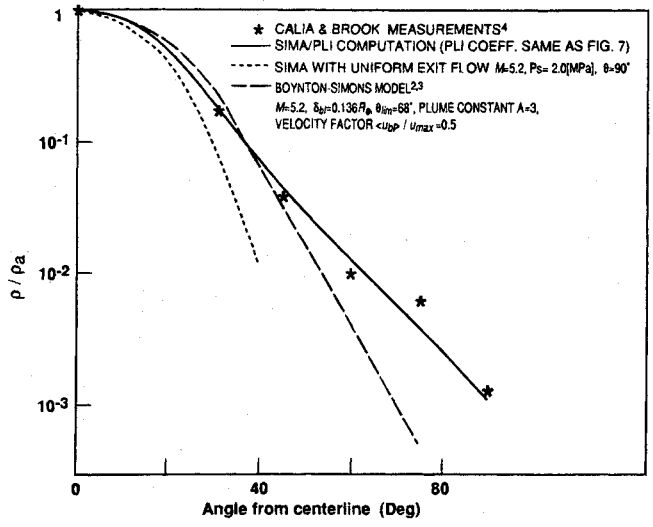

Fig. 8 Comparison of computed and measured density at polar radius of $92R_e$ ($\gamma = 1.37$).

and Boynton-Simons approximation. The measured variables were density and flow velocity, from which mass flux was obtained as the product of density and velocity. The experiments were performed in a vacuum chamber; the nozzle had a wall lip angle of $\theta_w = 80$ deg, an area ratio of 40:1 and 1.09 *mm* throat radius; the gas was nitrogen ($\gamma \approx 1.4$). The detectors were located on a circular arc centered at about the middle of the nozzle exit plane, and located at a radius of $92R_e$. In conforming to this geometry, we converted the display of our computations to show flow variables as function of angle from plume axis at polar distance of $92R_e$. At this high range, it was rightfully assumed by Calia and Brook that the measured flow velocity was the limiting flow velocity.

Considering the limiting velocity profile (Fig. 7), we note that at the relatively high angle of 90 deg, the limiting velocity was reduced to about one-half of its plume axis value. Our SIMA/PLI computation was matched to this measurement by setting $T_l/T_a = 0.25$ and $N_T = 4$. A close agreement of SIMA/PLI with mass flux measurement was obtained as well (Fig. 7). We have not presented computational results using uniform SIMA or Boynton-Simons in this case. Uniform SIMA assumes uniform stagnation temperature and hence is irrelevant to this experiment; the Boynton-Simons model does not contain a treatment of stagnation temperature.

Turning to the density profile (Fig. 8), a reasonable agreement is observed between SIMA/PLI density computation and measurements, over the relatively large range of 1–0.001 of the normalized density. Both the uniform SIMA and the Boynton-Simons model exhibit a clearly exaggerated rate of decay of the density with angle from plume axis. This observation indicates that the correction introduced as the PLI approximation to the exit plane nonuniform flow is by and large a good one. The ratio of nozzle lip stagnation density in the nonuniform and uniform computations is about 0.006. Even though the lip stagnation density is so much smaller in the nonuniform case, the density at a streamtube that turns by a high angle of nearly 90 deg is higher than the corresponding density in the uniform SIMA computation. This is interpreted as indicating that the dominant effect is not that of reduced stagnation density near the lip, but rather that of variation of Mach number as function of flow turning angle. Nonuniform streamtubes, starting at Mach numbers close to the sonic value at the lip, expand to lower Mach numbers at corresponding turning angles than uniform flow streamtubes. This is another indication supporting the arguments leading to the power-law approximation of exit plane Mach number.

To assess the sensitivity of the density and mass flux distributions to PLI coefficients, we conducted additional computations changing a single coefficient at a time as follows: $N_\theta = 1$, $N_M = 7$, $N_T = 5$, and $N_P = 9$. Negligible change in results was found in all instances, except Mach-number power which resulted in about 5% increase at large angles (above 45 deg). Changing to *uniform* exit pressure, i.e., $P_l = P_a$, we found some 10% increase in density for large angles (above 45 deg).

C. Comparison with Lengrand et al. Experiments

In Figures 9–11, the present computations are compared to corresponding axial and transverse density and temperature measurements of Lengrand et al.[5] The experiments were performed on nitrogen plumes generated by small nozzles mounted inside a vacuum chamber. The nozzle lip wall angle was $\theta_w = 80$ deg.

Considering first the variation of density and temperature along the plume axis (Fig. 9), we note that the density is well matched by the PLI computation, but there is a discrepancy factor of about 1.6 between the measurements and uniform SIMA computation. This mismatch indicates a correspondingly undervalued Mach number on the plume axis; it means that the uniform exit flow streamtubes diverge at below the actual rate, which is similar to our observation in the case depicted in Fig. 4 above. The temperature discrepancy (Fig. 9) is lower

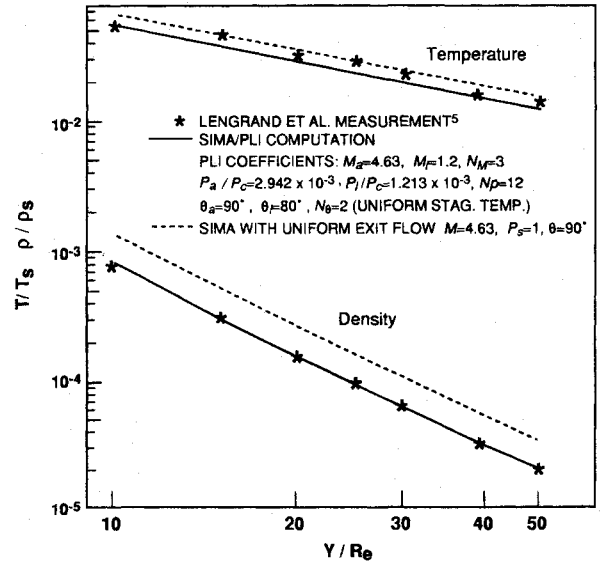

Fig. 9 Comparison of computed and measured density and temperature along plume axis ($\gamma = 1.4$).

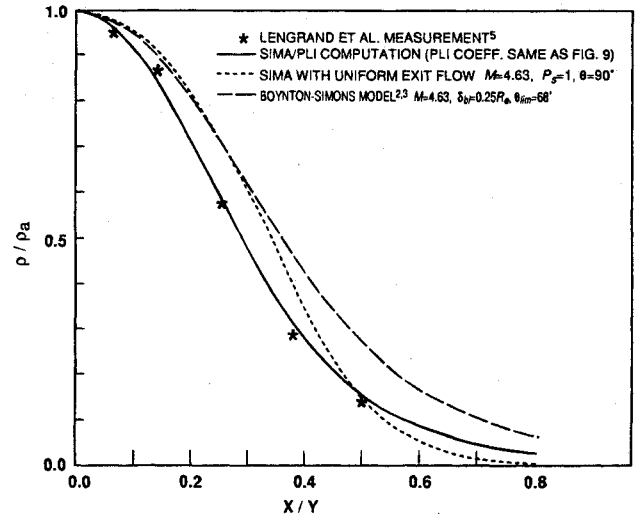

Fig. 10 Comparison of computed and measured density across the plume at $Y = 20R_e$ ($\gamma = 1.4$).

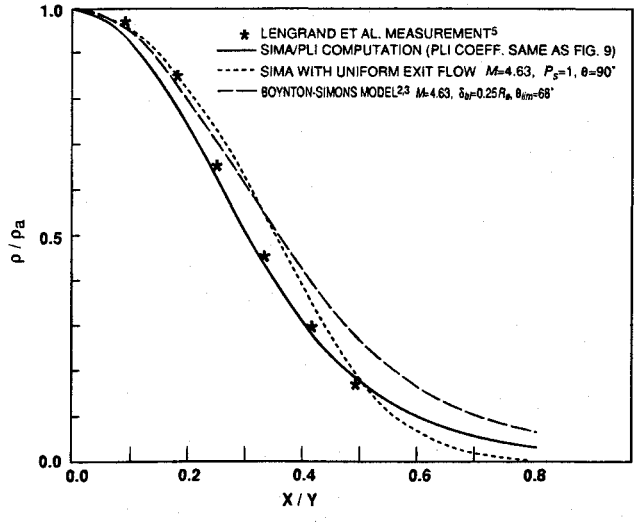

Fig. 11 Comparison of computed and measured density across the plume at $Y = 30R_e$ ($\gamma = 1.4$).

than that of the density by about the temperature-to-density adiabatic index of $\gamma - 1 = 0.4$.

The transverse density variations (at constant Y) are shown in Figs. 10 and 11 for $Y = 20R_e$ and $Y = 30R_e$, respectively. We observe that the PLI results are at a reasonable agreement with the measurements. The uniform SIMA and Boynton-Simons computations do not agree with the general trend exhibited by the measured density. The uniform computations exhibit an exaggerated decay rate at the intermediate range of $X/Y = 0.3$ to 0.5. The Boynton-Simons model generally yields an overvalued density at the range of $X/Y > 0.2$.

For a sensitivity check of the density and temperature distributions to PLI coefficients, we conducted additional computations changing a single coefficient at a time as follows: $N_\theta = 1$, $N_M = 4$, and $N_P = 10$. Negligible change in results was found in all instances, except Mach-number power which resulted in about 10% increase at the plume axis.

V. Conclusions

It has been demonstrated that the SIMA/PLI approach results in computations that agree well with measurements of exhaust plumes in an intermediate range (several times $10R_e$), both on-axis and off-axis. The process of adjusting PLI coefficients involves the determination of four major parameters, namely the axial exit Mach number as well as the powers for Mach number, pressure, and flow angle variations. The procedure of determining the PLI coefficients for stagnation temperature constitutes an independent uncoupled stage.

The axial Mach number was found to be slightly less than the nominal exit Mach number (based on geometrical area ratio), which agrees with the notion of effectively reduced exit area ratio due to viscous effects (boundary layer). Axial distributions of Pitot pressure or density were (predictably) found to be sensitive to the assumed axis Mach number M_a and also to the PLI Mach number power N_M. This provides a means for determination of both M_a and N_M from measured axial values of flow variables; our results seem to indicate that M_a thus determined is accurate to within about ± 0.1, and N_M is accurate to about ± 1.

When mass flow rate data is available, it may be incorporated into the coefficients determination scheme, improving the estimate of axial Mach number (and the power coefficient as well); it has not been done at the present stage of our SIMA/PLI method.

The PLI power coefficient for pressure was found to be relatively high, in the range of 10–12. This is a result of the way we define exit plane stagnation pressure as dependent on Mach number and static pressure. SIMA/PLI computations exhibited a relative insensitivity to changes of 1–2 units in the PLI pressure power coefficient. Even the drastic assumption of *uniform* exit pressure did not alter plume flow excessively. This demonstrates that the delicate lip-flow assumption [Eq. (11)] is not crucial to the validity of the SIMA/PLI methodology.

The power coefficient for Mach number was generally in the range of 3–4 in experiments using small nozzles[5,7], and had a larger value of 8 for the relatively larger nozzle of Ref. 4. This seems to correlate with the notion of higher PLI power corresponding to a thinner boundary layer, which is present at the larger nozzle.

The PLI power coefficient for flow angle was $N_\theta = 2$ in all three nozzles tested. This particular value implies a zero derivative of $\theta_e(X)$ at the axis ($X = 0$); so that the exit streamtube at the plume axis does not diverge at all. A sensitivity check revealed that density and Pitot pressure were insensitive to a change of power $N_\theta = 1$ at ranges above about $10R_e$.

A sensitivity study was conducted on all PLI coefficients. The main conclusion is that density and Pitot pressure are insensitive to all coefficients except M_a and N_M, particularly at ranges above about $10R_e$. This essentially demonstrates quantitatively a significant feature of plume flowfields—at intermediate and large range (above about $10R_e$) they are relatively insensitive to details of the exit plane flow; we interpret this result as follows. At large range, usually above $60R_e$, and at angles not far from the plume axis, the Boynton-Simons[2,3] point-source approximation provides a good description of the flow density. The PLI approximation of exit flow, using the gasdynamic reasoning that was incorporated in the model formulation, succeeded in capturing those features of nonuniformity in the exit flow that enable to obtain valid SIMA/PLI computations at the intermediate range of about $10R_e$ to $60R_e$. In addition, the SIMA/PLI results at large angles to the plume axis agree with experiments better than the Boynton-Simons[2,3] model.

As a concluding remark, we suggest that the combination of an exit plane flow approximation (PLI) and an accurate MOC scheme (SIMA) renders a better computational method for small plumes at intermediate range, than either the classical Boynton-Simons[2,3] analytic approximation or a MOC computation based on uniform exit flow. Moreover, when measurements of stagnation temperature in a plume are available, the PLI can be adjusted to match them fairly well, while Boynton-Simons model does not treat stagnation temperature.

References

[1] Dettleff, G., "Plume Flow and Plume Impingement in Space Technology," *Progress in Aerospace Science,* Vol. 28, No. 1, 1991, pp. 1–71.

[2] Boynton, F. P., "Exhaust Plumes from Nozzles with Wall Boundary Layers," *Journal of Spacecraft and Rockets,* Vol. 5, No. 10, 1968, pp. 1143–1147.

[3] Simons, G. A., "Effect of Nozzle Boundary Layers on Rocket Exhaust Plumes," *AIAA Journal,* Vol. 10, No. 11, 1972, pp. 1534–1535.

[4] Calia, V. S., and Brook, J. W., "Measurements of a Simulated Rocket Exhaust Plume Near the Prandtl-Meyer Limiting Angle," *Journal of Spacecraft and Rockets,* Vol. 12, No. 4, 1975, pp. 205–208.

[5] Lengrand, J.-C., Allègre, J., and Raffin, M., "Experimental Investigation of Underexpanded Exhaust Plumes," *AIAA Journal,* Vol. 14, No. 5, 1976, pp. 692–694.

[6] Dettleff, G., Boettcher, R. -D., Dankert, C., Koppenwallner, G., and Legge, H., "Attitude Control Thruster Plume Flow Modelling and Experiments," AIAA Paper 85-0933, Williamsburg, VA, June 1985.

[7] Legge, H., and Dettleff, G., "Pitot Pressure and Heat Transfer Measurements in Hydrazine Thruster Plumes," *Journal of Spacecraft and Rockets,* Vol. 23, No. 4, 1986, pp. 357–362.

[8] Legge, H., "Shear Stress and Pressure in Plume Impingement Flow," *Proceeding of the 15th International Symposium on Rarefied Gas Dynamics,* Grado, Italy, edited by V. Boffi and C. Cercignani, Vol. I, B. G. Teubner, Stuttgart, 1986, pp. 523–538.

[9] Hill, J. A. F., and Draper, J. S., "Analytical Approximation for the Flow from a Nozzle into Vacuum," *Journal of Spacecraft and Rockets,* Vol. 3, No. 10, 1966, pp. 1552–1554.

[10] Dettleff, G., "A Study of Rocket Exhaust Plumes and Impingement Effects on Spacecraft Surfaces. II. Plume Profile Analysis. Method of

Characteristics Computer Program for Axisymmetric Free Jets. Part 3: Extended version 'Free Jet'." DLR Internal Rep. IB 222-82 A 07, Göttingen, 1982.

[11] Hoffman, R. J., Kawasaki, A., Trinks, H., Bindemann, I., and Ewering, W., "The CONTAM 3.2 Plume Flowfield Analysis and Contamination Prediction Computer Program: Analysis Model and Experimental Verification," AIAA Paper 85-0928, Williamsburg, VA, June 1985.

[12] Boynton, F. P., "Highly Underexpanded Jet Structure: Exact and Approximate Calculations," *AIAA Journal,* Vol. 5, No. 9, 1967, pp. 1703–1704.

[13] Cline, M. C., "VNAP2: A Computer Program for Computation of Two-Dimensional, Time-Dependent, Compressible Turbulent Flow," Los Alamos National Lab., LA-8872, Los Alamos, NM, Aug. 1981.

[14] Bird, G. A., "Breakdown of Continuum Flow in Free Jets and Rocket Plumes," *Proceeding of the 12th International Symposium on Rarefied Gas Dynamics,* edited by S. Fisher, Vol. 74, AIAA, New York, 1981, pp. 681–694.

[15] Hueser, J. E., Melfi, L. T., Bird, G. A., and Brock, F. J., "Rocket Nozzle Lip Flow by Direct Simulation Monte Carlo Method," *Journal of Spacecraft and Rockets,* Vol. 23, No. 4, 1986, pp. 363–367.

[16] Zucrow, M. J., and Hoffman, J. D., *Gas Dynamics,* Vol. II, John Wiley, New York, 1977.

[17] Falcovitz, J., and Fuhs, A. E., "A Semi-Inverse Marching Characteristics Scheme for Supersonic Flows," *AIAA Journal,* Vol. 30, No. 4, 1992, pp. 1128–1130.

[18] Bird, G. A., "The Nozzle Lip Problem," *Proceeding of the 9th International Symposium on Rarefied Gas Dynamics,* edited by M. Becker and M. Fiebig, Vol. I, DFVLR Press, 1974, pp. A22.1–A22.8.

[19] Smith, S. D., "Improvement of Rocket Engine Plume Analysis Techniques," Final Rep., Lockheed Huntsville Research & Engineering Center, LMSC-HREC TR D784753, Jan. 1982; See also NASA-CR-167516.

James A. Martin
Associate Editor